ORIGINAL RESEARCH

The effects of network reinforcement distribution on the mechanical properties and cutting behavior of SiCp/Al composites

Liangfei Hu[1] · **Xu Zhang**[1] · **Chaoyu Xie**[1] · **Xuechang Zhang**[2] · **Jie Shen**[3]

Abstract

The morphology and distribution structure of the reinforcement have a significant effect on the mechanical properties and cutting process of composites. In this paper, two-dimensional tensile and cutting models are established respectively, and the validity of the models is verified by comparing with the cutting force and chip morphology in the experiment. The effects of network reinforcement distribution and particle aspect ratio on the mechanical properties and surface quality of SiCp/Al composites were compared and analyzed. Results show that the aggregation of particles can enhance their continuity, thereby improving their bearing capacity. Network structures and the increase in aspect ratios of particles both can enhance the degree of aggregation of particles, thereby improving their bearing capacity. However, an increase in the degree of aggregation of particles will also lead to an increase in cutting forces and a deterioration in surface quality. The hybrid network structure of particles with different aspect ratios was proposed. Compared with the ellipse particle reinforced network composites model, the network structure with hybrid particles improved the surface quality by 41.7%, while ensures the strengthening effect of the composite material.

Keywords SiCp/Al composites · Network distribution · Aspect ratio · Hybrid particle · Mechanical properties · Machined surface quality

Introduction

The demand for new and high-performance materials in various industries is increasing as science and technology advance. MMCs (Metal Matrix Composites) are widely used in automotive, aerospace, and other fields due to their high strength and lightweight [1–3]. The addition of reinforcing phase to the aluminum matrix is often used to improve its mechanical properties [4, 5]. According to research, the strengthening effect of MMCs is related to the inherent parameters of the reinforcement as well as the distribution state of the reinforcement. The properties of discontinuously reinforced MMCs are superior to those of uniformly distributed composites [6]. Due to the breakdown of the integrity of the matrix elements, uniformly distributed composites have limited plasticity. In contrast, the complete matrix element is kept in MMCs with network reinforcement distribution, and the plasticity of the matrix element is considerably exerted, enhancing the strength and plasticity of the composites [7]. Kumai et al. [8] discovered that by preparing SiCp/A356 network composites, cracks in network structure can be easily deflected and closed. Huang et al. [9] used the reaction hot pressing process to prepare TiB whiskers (TiBw)/Ti-6Al-4 V composites with a novel network distribution and dendritic morphology, which is believed to be favorable for load transmission in composite materials. The tensile strength of the prepared TiBw/Ti-6Al-4 V composites is significantly higher than that of Ti-6Al-4 V alloys. Kaveendran et al. [10] developed composites (Al2O3 + ZrAl3)/Al networks. Tensile strength increased by 12.5% and elongation increased by 76.9% when compared to composites with uniform reinforcement distribution. Gao et al. [11] have established a three-dimensional model with a network structure and conducted numerical studies on its reinforcement and

✉ Liangfei Hu
liangfei_hu@163.com

1 School of Mechanical and Automotive Engineering, Shanghai University of Engineering Science, Shanghai 201620, China

2 School of Mechanical and Energy Engineering, NingboTech University, Ningbo 315100, China

3 College of Engineering and Computer Science, University of Michigan-Dearborn, Dearborn, MI 48128, USA

fracture behavior. The results indicate that metallic matrix composites (MMCs) with quasi-continuous network structures exhibit higher rigidity and strength than uniformly distributed composite materials. Slipenyuk et al. [12] used powder metallurgy to create AlCuMn/SiC/15p composites. While an increase in particle size ratio (PSR) can encourage reinforcement aggregation to form a network structure, excessive particle aggregation reduces composite workability and strength. This demonstrates the significance of properly managing the local volume fraction and reinforcement distribution in network composites structural design.

However, while reinforcements improve the mechanical properties of composites, they also make machining more difficult. There is significant tool wear and poor machined surface quality in the cutting process of SiCp/Al, as with other commonly used MMCs [13, 14]. Network composites have a more complex structure than uniform composites, and the reinforcements at the network boundary are densely distributed, which will affect cutting performance. Furthermore, studying the cutting process of network composites can provide feedback for the structural design of the composites and further improve the structure that is not conducive to the cutting process, allowing network composites to achieve better surface quality while maintaining excellent mechanical properties. As a result, research into network composites cutting is required.

The finite element method is increasingly being used to study the mechanical behavior and cutting process of composites. The finite element model of SiC particle-reinforced MMCs is developed by GENI et al. [15]. They discovered that the volume fraction, aspect ratio, and non-uniform distribution all have a significant impact on the fracture behavior and stress-strain relationship. Mishnaevsky et al. [16] established models of SiCp/Al with different microstructures to study the effects of volume fraction, size, and arrangement of SiC particles on flow stress and damage evolution. Gao et al. [11] developed a three-dimensional model of SiCp/6061Al network composites and discovered that as PSR increased, particle lode-carrying capacity increased but composites elongation decreased. Simultaneously, the PSR threshold with a good strengthening effect is provided. Dai et al. [17] proposed a SiCp/Al hybrid composites model, and found that multi-size not only improves the uniformity of the stress distribution but also improves the machined surface quality of the composites. Zhou et al. [18] developed 2024 Al-based composites reinforced with ZrC particles and/or Ni-coated carbon fibers, which were named Cf(Ni)-ZrC/2024 Al, ZrC/2024 Al, and Cf(Ni)/2024 Al, respectively. They also conducted tensile tests on these three types of samples, and the results indicated that the dual-enhanced bodies had better strengthening properties than the single-enhanced bodies, which could primarily be attributed to dislocation strengthening and load-transferring effects. The studies above show that, in addition to the size

and aspect ratio of the reinforcement, the hybrid distribution of particles is an effective way to improve composites performance.

However, most network composites are currently developed by adding a single reinforcement, ignoring the impact of hybrid reinforcements with different parameters on the strengthening effect of network composites, particularly hybrid reinforcements with different aspect ratios. As a result, this paper conducts extensive research on this topic. There have been numerous studies on the cutting simulation of SiCp/Al. Ghandehariun et al. [19] used the established multiphase model to predict particle failure modes and tool-particle interactions during the cutting of MMCs. Teng et al. [20] used a two-dimensional model to investigate the effects of tool rake angle and tool-particle position on the cutting behavior of SiCp/Al. The milling model of SiCp/Al is developed by Jin et al. [21], the results show that the particle removal mode changes due to the cutting position of the tool, and there are defects on the machined surface such as micro cracks and pits. Through experiments and the finite element method, Zhang et al. [22] investigated the effect of particle size and cutting speed on the cutting behavior of SiCp/Al. Saini et al. [5, 23–25] discovered that the occurrence of hard reinforcement in base Al-alloy makes the MMC difficult to machine. But machining turns relatively easier at high cutting speed and low feed rate, causing improved surface finish. As shown above, the parameters and distribution of reinforcements have a significant impact on the cutting performance of MMCs. There have been few studies on the cutting of network composites to date, and the removal mechanism of reinforced particles with network distribution requires further investigation using the finite element method. As a result, this paper investigates the cutting process of SiCp/Al network composites further based on the study of mechanical properties. A new network structure is proposed to improve the strength of SiCp/Al composites while making it have good processing surface integrity.

The Voronoi algorithm is used to create two-dimensional tensile and orthogonal cutting models of SiCp/Al with random distribution and network distribution using the ABAQUS/Explicit 2020 software. Through comparative analysis, the effects of aspect ratio and particle hybridity on the tensile stress of SiCp / Al composites with network distribution were studied. Following that, the machining removal mechanism, cutting force characteristics, and machined surface quality of network composites are thoroughly investigated.

Modeling of SiCp/Al network composites

Modeling steps

The typical microstructure of SiCp/Al with network reinforcement distribution is shown in Fig. 1(a). The network

structure is composed of reinforcement aggregation area and matrix area, and the reinforcement is randomly distributed in the network boundary. The structure is made of Al particles and SiC particles by vacuum hot pressing technology. Small SiC particles are distributed around large Al particles. The schematic diagram of the mixed powder is shown in Fig. 1(b). The hybrid particle reinforced network SiCp/Al can also be formed by hot pressing sintering of Al particles with hybrid SiC particles of different shapes or sizes.

The material parameters of the workpiece are kept constant while the particle distribution structure is changed based on the random SiCp/Al model in order to study the properties of the network SiCp/Al using the finite element method. SiC particles are simplified into circular and elliptical shapes because these shapes can fully and specifically characterize particle crack propagation and particle-matrix interface debonding.

The method of Zhao et al. [27] is used to generate SiCp/Al with network reinforcement distribution. To begin, a random Tyson polygon (Fig. 2(b)) is generated in ABAQUS finite element software using the Voronoi algorithm, and the network boundary of the polygon is expanded to a network layer with a width of 45 μm (Fig. 2(c)). Following that, SiC particles with a diameter of 15 μm are randomly inserted into the network layer, and a zero-thickness cohesive element is inserted as the interface phase between SiC and Al, forming a two-dimensional model of SiCp/Al with a quasi-continuous network structure, as shown in Fig. 2(f). The Al particles, network layer, SiC particles, and interface phase are visible in the SiCp/Al network composites models. In the composites model with random distribution, the overall volume fraction V_C of SiC is 18%. The local volume fraction V_L of SiC in the network layer describes the particle aggregation degree. V_L is defined in this paper as the ratio of the area of all particles to the network layer. The V_L calculation formula is as follows:

$$V_L = \frac{S_P}{S_N} = \frac{S_T \times V_C}{S_N} \tag{1}$$

where S_P, S_N, and S_T represent the particle, network layer, and overall model areas, respectively.

The model of SiCp/Al network composites

The cutting behavior of network composites is closely related to their mechanical properties. The study of mechanical properties can be used to explain the rationality of the structural design of network composites, laying the groundwork for the study of cutting behavior. As a result, tensile finite element models of SiC particles with network distribution are developed to investigate the effects of particle aspect ratio on the mechanical properties of network SiCp/Al. Four two-dimensional models are developed to simulate the tensile process of composites in order to investigate the effects of network particle distribution on the strengthening and fracture of SiCp/Al. Particles are also randomly distributed in the network layer in network composites. The area and equivalent diameter of elliptical particles are the same as those of circular particles, and the aspect ratio is 3:1. The volume fractions of circular and elliptical particles are roughly equal in the HPRNC model (Fig. 3(d)). The workpiece model has a size of 405 μm × 405 μm, and the specific parameters are shown in Table 1. The mesh density of Al and SiC is 2 μm, and the mesh unit is CPE4R. COH2D4 is the mesh unit of the cohesive element. The left side of the workpiece is fixed, and the right side is displaced 14 μm along the x axis. The tensile strain ε_x is approximately 3.46%. In the tensile process, particle fracture is ignored, and only the failure process of matrix material and interface phase is studied.

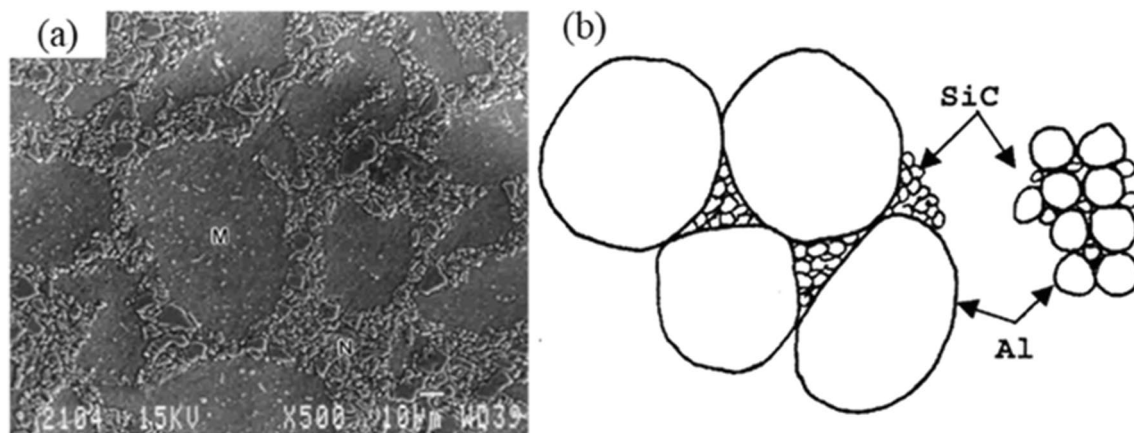The two-dimensional models considering particle fracture are established based on the above models to study the

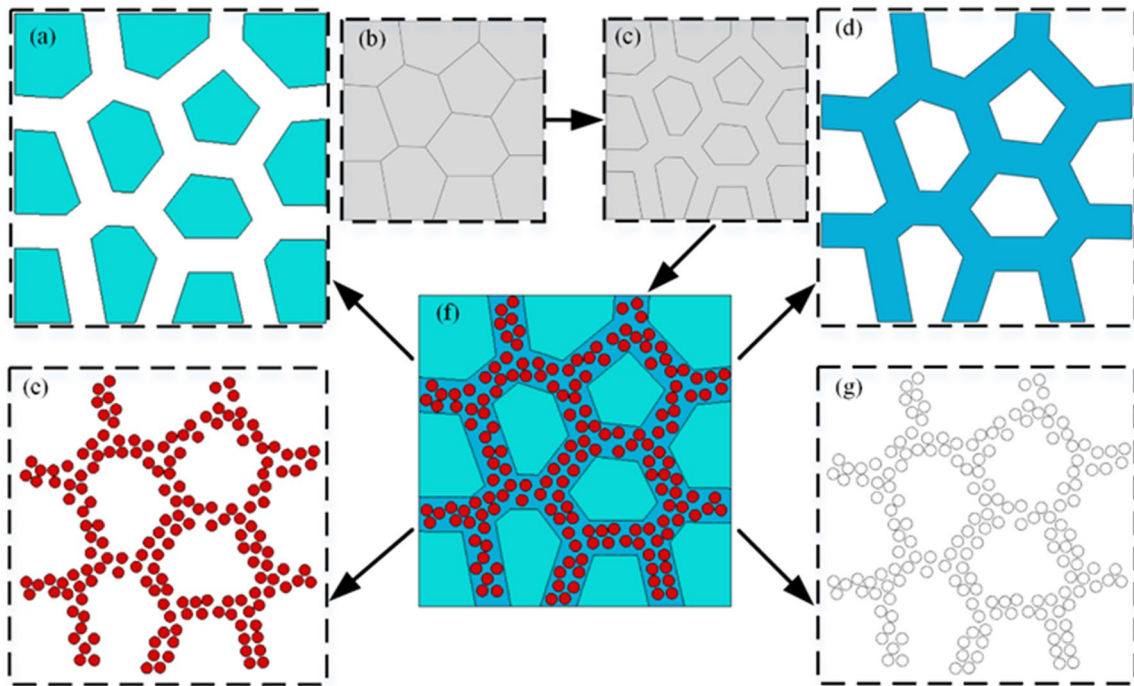**Fig. 1** Typical Microstructure of network SiCp/Al [26]: (**a**) SEM images and (**b**) schematic diagram of the mixed powder

Fig. 2 The structural properties of network SiCp/Al: (**a**) Al particles, (**b**) Tyson polygon, (**c**) Widening network boundary, (**d**) Network layer, (**e**) SiC particles, (**f**) finite element model, and (**g**) cohesive element

Fig. 3 Tensile models of SiCp/Al: (**a**) random model, (**b**) circular particle reinforced network composites (CPRNC) model, (**c**) ellipse particle reinforced network composites (EPRNC) model, and (**d**) hybrid particle network (HPRNC) model
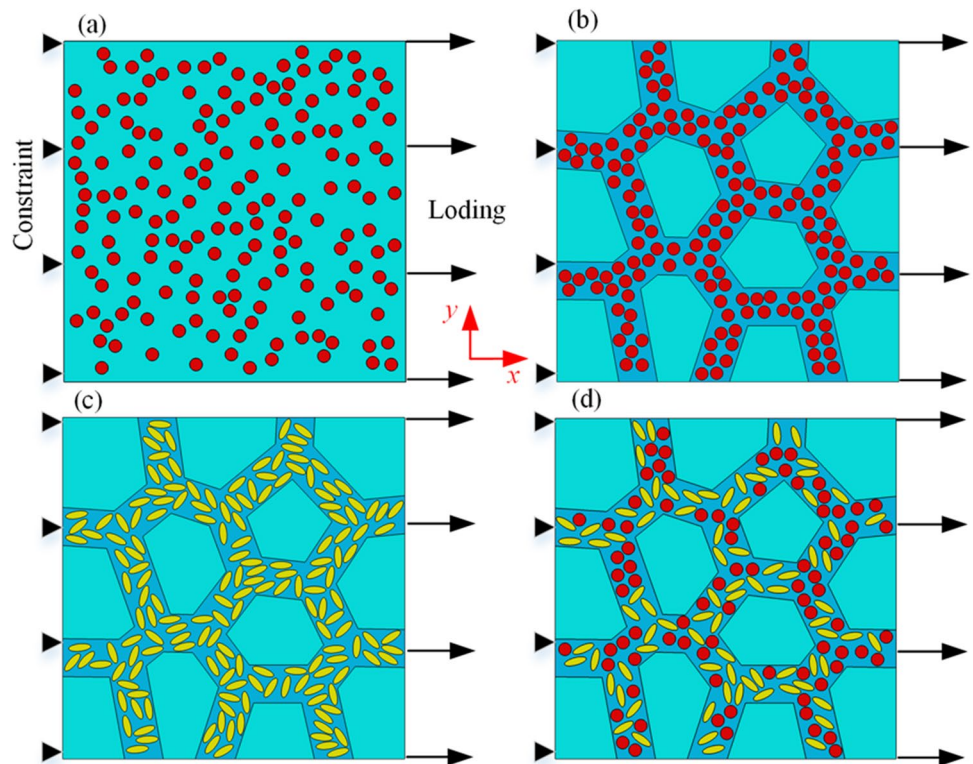
effects of network particle distribution on the cutting process of SiCp/Al, and the parameters of the workpiece model are kept unchanged, as shown in Fig. 4. The side and bottom of the workpiece are fixed to limit the movement of the workpiece. PCD tool is set as rigid body during cutting, and the tool parameters are shown in Table 1.

Table 1 Cutting parameters in finite element models [28]

Parameters	Values
Cutting speed (mm/min)	1200
Volume fraction (%)	18
Particle size (μm)	15
Tool rake angle (°)	3
Tool clearance angle (°)	7
Cutting edge radius (μm)	5

Materials properties

The plastic behavior of the metal matrix composite is described using the Johnson-Cook model. Whichcan be represented by:

$$\sigma_{JC} = \left[A + B(\varepsilon)^n\right]\left[1 + C\ln\left(\frac{\dot{\varepsilon}}{\dot{\varepsilon}_0}\right)\right]\left[1 - \left(\frac{T - T_{room}}{T_{melt} - T_{room}}\right)^m\right] \tag{2}$$

where σ_{JC} represents equivalent flow stress, ε represents equivalent plastic strain, $\dot{\varepsilon}$ represents equivalent plastic strain rate, and $\dot{\varepsilon}_0$ represents reference plastic strain rate. T denotes the workpiece's temperature. T_{room} and T_{melt} denote the reference temperature and melting temperature, respectively. The strain hardening coefficient of the material is denoted by A, B, and n. The strain rate hardening coefficient is C, and the thermal softening coefficient is m. The separation criterion of Al2024 is the Johnson-Cook(J-C) fracture criterion [29]. The ductile fracture criterion [30] is used to judge the initial damage in order to predict the fracture behavior of aluminum matrix during the tensile process. The fracture energy method [31] is used to characterize the stress-strain relationship of a material after it has been damaged. Table 2 displays the mechanical parameters of Al2024 as well as the parameters of the J-C model.

To simulate the damage evolution of SiC during the cutting process, the maximum normal stress criterion [32] is used to determine fracture stress after particles undergo elastic deformation under load. The fracture energy criterion governs how damage evolves after particle fracture. Table 3 shows the brittle fracture parameters.

The cohesive element is used to describe the SiC-Al interface stress transfer and debonding process. The failure process is governed by the bilinear traction separation

Fig. 4 Cutting models of SiCp/Al: (**a**) random model, (**b**) CPRNC model, (**c**) EPRNC model, and (**d**) HPRNC model
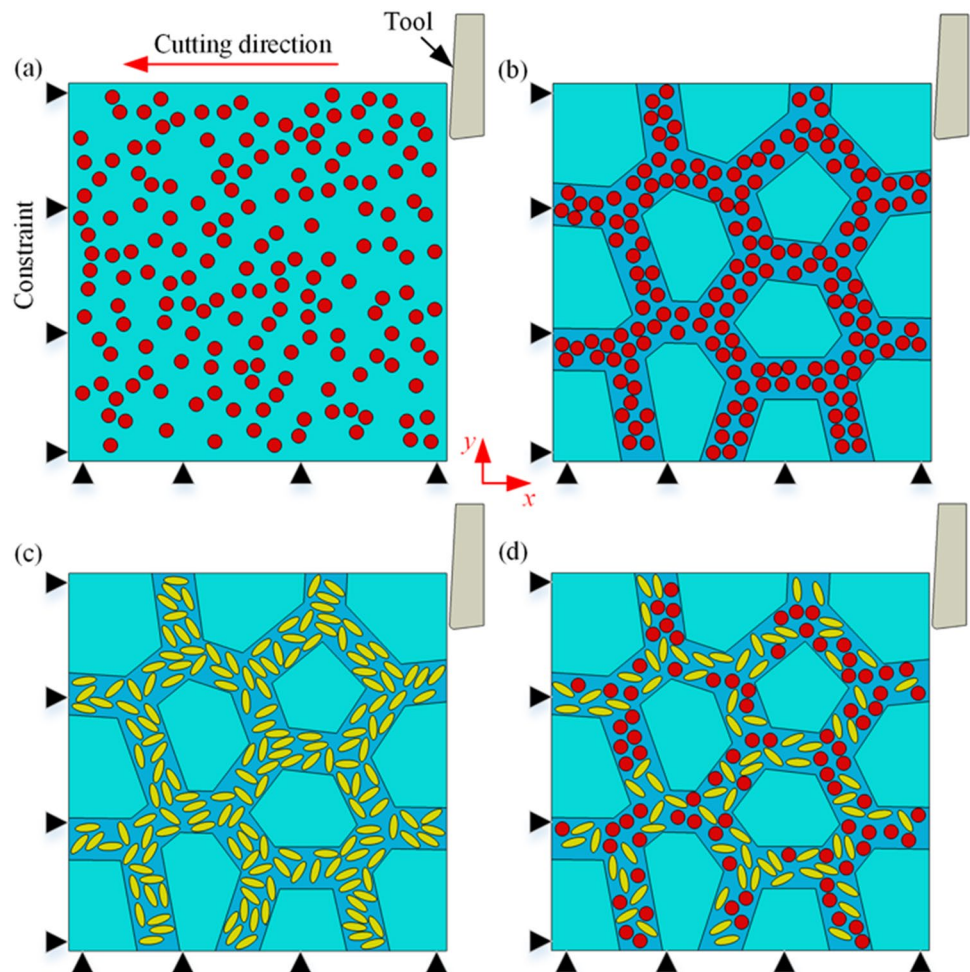
Table 2 Mechanical properties and J-C model parameters of Al2024 [20]

Parameters	Values
Density(g/cm^3)	2.77
Elastic modulus (MPa)	73,000
Poisson's ratio	0.33
Thermal conductivity (W/(m•K))	190
A (MPa)	352
B (MPa)	440
n	0.42
m	1
C	0.0083
d_1	0.13
d_2	0.13
d_3	−1.5
d_4	0.011
d_5	0

Table 3 Mechanical parameters and brittle fracture parameters of SiC [29, 33]

Parameters	Values
Density(g/cm^3)	3.13
Elastic modulus (MPa)	420,000
Poisson's ratio	0.14
Thermal conductivity (W/(m•K))	81
σ_0(MPa)	1500
G_f^I(J/m^2)	30
p	1
ε_{max}^{ck}	0.001

law. The cohesive element begins to fail when the stress reaches the maximum nominal stress [29]:

$$\max\left\{\frac{\langle\sigma_n\rangle}{\sigma_n^0}, \frac{\sigma_s}{\sigma_s^0}\right\} = 1 \tag{3}$$

where σ_n and σ_s are the normal and tangential components of stress. σ_n^0 and σ_s^0 are the maximum nominal normal and tangential stress. When the initial damage criterion is reached, the stiffness of the cohesive element will begin to decay according to the damage coefficient D. The calculation formula of D is as follows:

$$D = \frac{\delta_m^f\left(\delta_m^{max} - \delta_m^0\right)}{\delta_m^{max}\left(\delta_m^f - \delta_m^0\right)} \tag{4}$$

where δ_m^0 is the effective displacement at initial damage, δ_m^f is the effective displacement at the complete failure of the interface, and δ_m^{max} is the maximum effective displacement during loading. The stiffness K_i of the interface layer is:

$$K_i = K_i^0(1 - D) \tag{5}$$

where K_i^0 is the stiffness when the interface layer is intact, which includes normal stiffness K_n^0 and tangential stiffness K_s^0. When $D = 1$, that is, $\delta_m^{max} = \delta_m^f$, the stiffness K_i of the interface layer decreases to 0, and the cohesive element fails. The fracture energy of the cohesive element G^C is the area of the tension-displacement curve used to determine the failure process of the cohesive element:

$$G^C = \frac{1}{2}\left(\sigma_{max} * \delta_m^f\right) \tag{6}$$

where σ_{max} is the interface strength.

Model verification

To validate the models, cutting simulations were performed at cutting depths of 0.02 mm, 0.03 mm, and 0.04 mm, and the findings were compared to the experimental results. As shown in Fig. 5, the relative error between the random model and the experiment varies with cutting depth, with the highest relative error being 12.8%, showing that the simulation results are in good agreement with the experimental results. Furthermore, as shown in Fig. 5, the average cutting force of the network models is greater than that of the random model, but it is still less than the actual value of the random model. The average cutting force trend of the network model is consistent with changing cutting depth, indicating that the network models can accurately anticipate the cutting process.

Figure 6 shows the comparison between the experimental and simulated chip morphology of SiCp/Al at a cutting depth of 0.02 mm. As shown in Figs. 6(a)–(c), the chips of SiCp/Al are serrated, and there are defects such as micro-cracks and particle breakage in the chips. In addition, the presence of SiC particles makes chips easy to fracture and separate, thus forming staged serrated chips. Similar chip morphology is observed in the finite element models under the same cutting parameters, as shown in Figs. 6(d)–(g). The chips are mixed with particles that have been broken down by extrusion. At the same time, the chips exhibit serrated characteristics along the shear band. This demonstrates that the material parameters specified in the models are correct. For the network model, when the tool passes through the network area, due to a large number of particles, the chips are more easily separated during the formation process, resulting in a decrease in chip continuity.

SSD depth is a measurement of the depth of defects beneath a machined surface. As shown in Fig. 7(a) and (c), SSD is caused by defects such as pits and voids below the machined surface. In the finite element model, the
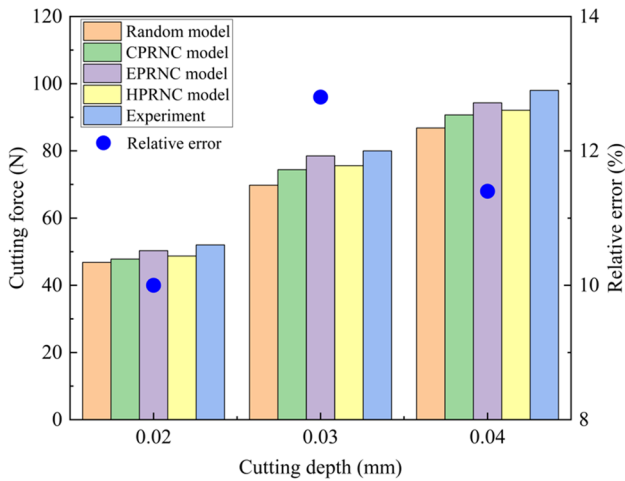
Fig. 5 Comparison of cutting force between simulation and experiment [20]

defect depths of the voids and cavities are 8.9 m, 8.4 m, and 8.5 m, respectively, and are marked with a red dotted box in Fig. 7(b). The final SSD depth is determined by taking the average depth of the three defects and comparing it to the experimental results. The relative error between the simulated and the experimental results is 9.5%, as shown in Fig. 7(d). Compared with the random model, the network

model only changes the distribution structure of particles, and other parameters are the same. Therefore, the verification of the random model can indirectly explain the accuracy of the network model in predicting surface quality.

To sum up, under the same workpiece and cutting parameters, the accuracy of the finite element model is proved by comparing the simulated cutting force, thrust, chip shape, and SSD depth with the experimental results, and the error between the simulation and the experimental results is within a reasonable range.

Results and discussion

Effects of network particle distribution on mechanical properties of SiCp/Al

Figure 8 shows the loading state of SiC particles when $\varepsilon_x = 1\%$. The stress of SiC in the tensile process of the two types of composites is greater than that of the matrix, so reinforced particles are critical to improving the lode-bearing capacity. As shown in Fig. 8(a), the stress distribution of particles in the random model is uniform. In network composites, there is obvious stress concentration on SiC in the network layer, and the stress is higher than in the random model. This is due to the high continuity of the particles in
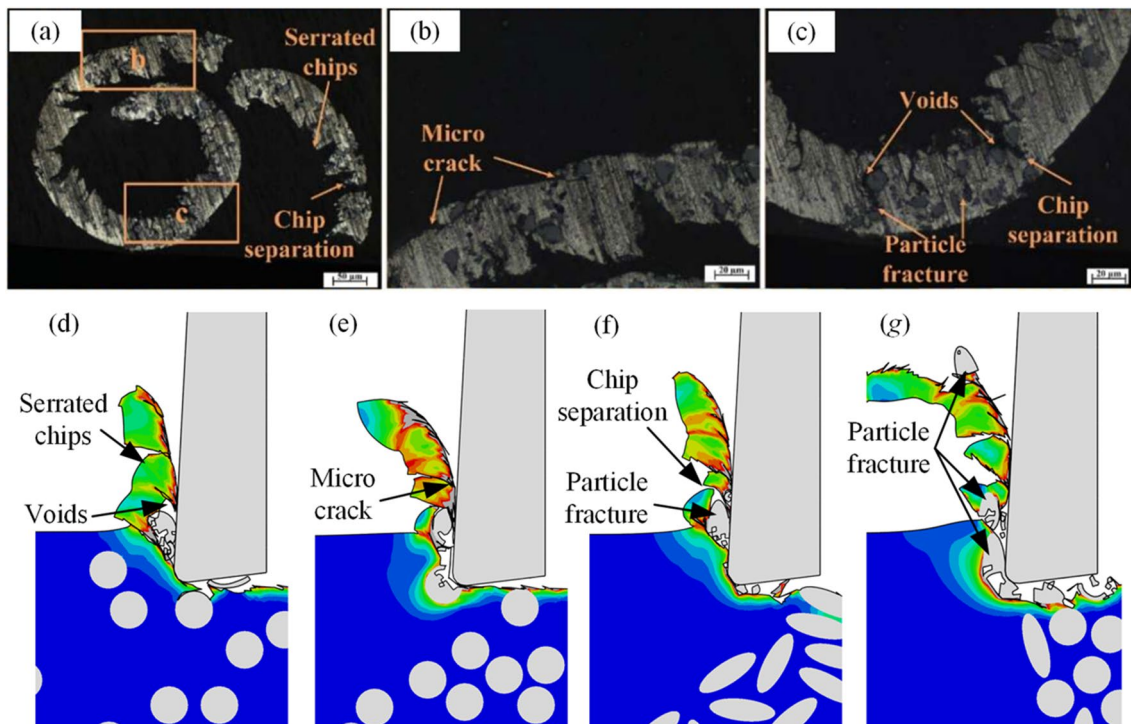

Fig. 6 Comparison of chip morphology between simulation and experiment [20]: (**a**), (**b**), (**c**) SEM photos of experimental chip, (**d**) random model, (**e**) CPRNC model, (**f**) EPRNC model, and (**g**) HPRNC model
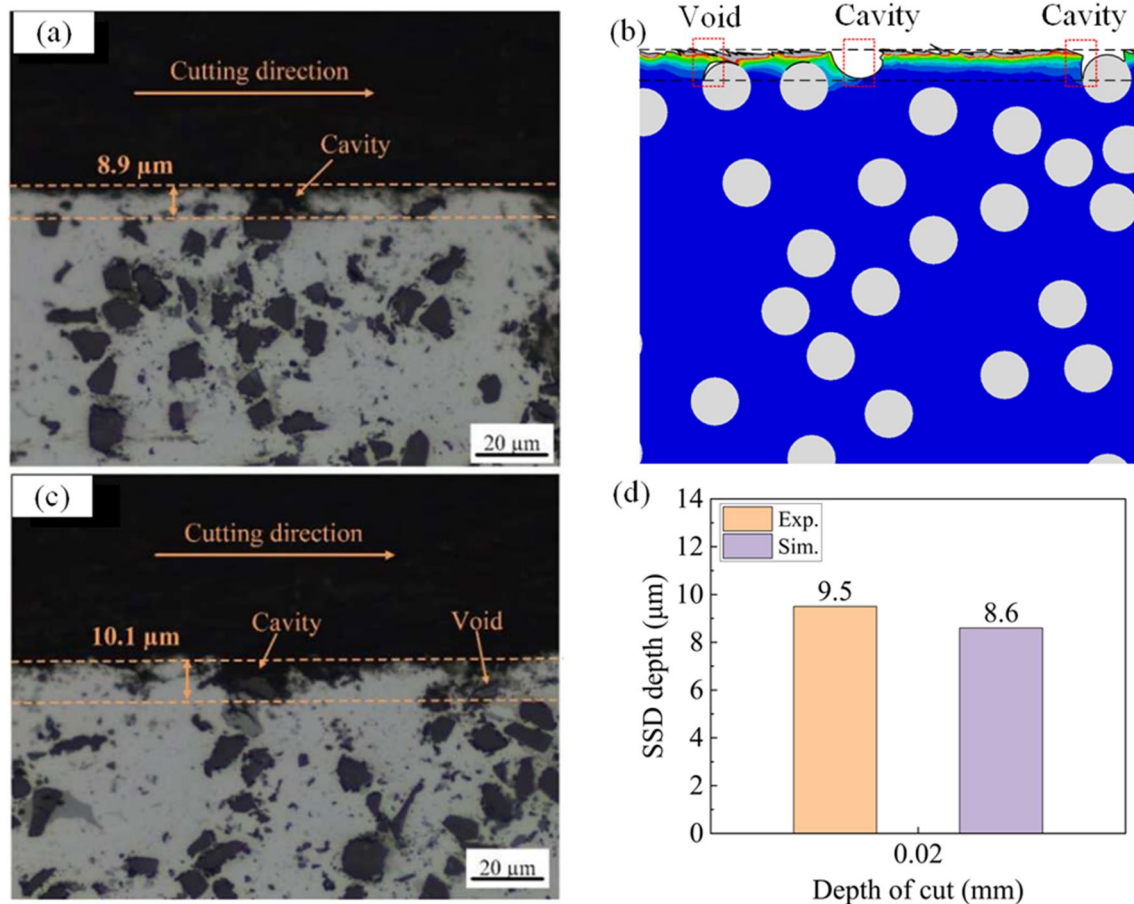
Fig. 7 Comparison of simulated and experimental [20] results at a cutting depth of 0.02 mm in a random model (**a**) SSD depth measured for the first time in the experiment, (**b**) SSD depth measured in the model, (**c**) SSD depth measured for the second time in the experiment, and (**d**) comparison of simulated and experimental SSD depths

the network layer, which allows the stress generated during the tensile process to be more easily transferred to the particles.

The particles arranged in the horizontal direction have high continuity in the CPRNC model (Fig. 8(b)), so the ability to bear load is high. The stress of particles increases significantly in the EPRNC model (Fig. 8(c)) as the aspect ratio of the particles increases, and the maximum stress exists in the particles along the tensile direction of the long axis, and the maximum stress reaches 909.1 MPa. It can be seen that increasing the aspect ratio of particles improves their load-bearing capacity, and the load-bearing capacity is related to the angle between particles and the tensile direction. The greater the angle, the greater the load. On one hand, the continuousness of particles in the network structure increases after the addition of elliptical particles, enhancing the interaction between particles. Metal internal stresses are more easily transferred to particles, resulting in particle stress concentration. On the other hand, elliptical particles have a longer interface and are subject to stress primarily from

the top and bottom directions, so metal internal stresses are more readily transferred to horizontal elliptical particles. Additionally, when a crack reaches a particle, the particle prevents the expansion of the crack until it breaks or debonds. Since the strength of particles is much greater than the interfacial strength, debonding always occurs before particle failure, and typically along the interface. When a crack encounters an elliptical particle, it extends over a longer distance, consuming more energy, and making it less likely to occur. Therefore, both the EPRNC model and the HPRNC model can handle higher loads. Furthermore, because the network layer has a constant width, increasing the aspect ratio reduces the distance between elliptical particles, resulting in significant particle stress concentration in a small range of the EPRNC model, as shown in Fig. 8(c). However, this may cause the particles to fracture prematurely. The stress level of particles in the HPRNC model decreases as the number of elliptical particles decreases, as shown in Fig. 8(d). Simultaneously, the hybrid distribution of circular and elliptical particles increases the distance between
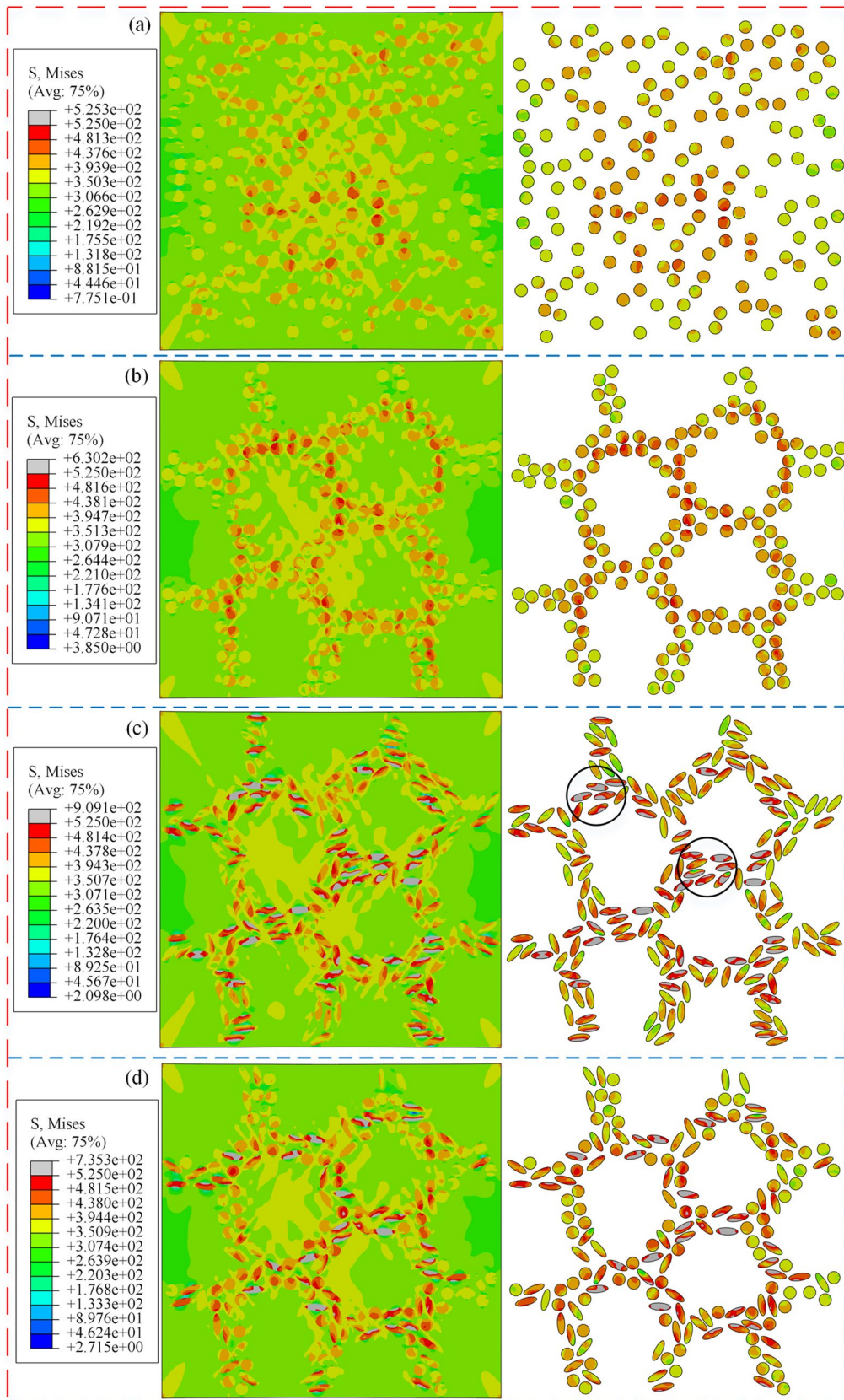
Fig. 8 Lode-bearing state of SiC particles in SiCp/Al ($\varepsilon_x = 1\%$): (**a**) random model, (**b**) CPRNC model, (**c**) EPRNC model, and (**d**) HPRNC model

elliptical particles and uniformizes the particle distribution, resulting in no significant stress concentration in the composites. The overall stress distribution of particles is more uniform than in the EPRNC model, lowering the risk of particle fracture.

As shown in Fig. 9, the average stress is used to quantitatively evaluate the carrying capacity of SiC particles. The typical stress relationship of particles in the small tensile deformation range is EPRNC model > HPRNC model > CPRNC model > random model. As can be seen, raising the aspect ratio strengthens the network composites. At the same time, as shown at A, the particles of the HPRNC model can still maintain a high stress level at 1.5% strain, and the average stress is slightly different from the EPRNC model, indicating that the distribution structure with hybrid particles can also better maintain the load-bearing effect of the network composites. The stress curve of the network models decreases quicker than the random model. Because the local volume fraction of the network models is greater (39%), more stress is generated in the network layer, resulting in premature damage to the composites. Furthermore, in the EPRNC model, the stress curve of the particles dropped the earliest, suggesting that the composites were damaged earlier and the elongation decreased. At B, the stress level of the HPRNC model gradually declines because the plastic matrix material slows crack propagation, suggesting that the network structure with hybrid particles can better exploit the plastic advantage of the matrix.

In summary, the aspect ratio and particle hybridity have a significant impact on the properties of SiCp/Al. Increasing the aspect ratio can increase particle bearing capacity, but it will cause premature damage to the composite substance. The HPRNC model can sustain a high stress level, indicating that the network structure composed of circular and elliptical particles can improve the network SiCp/Al performance.
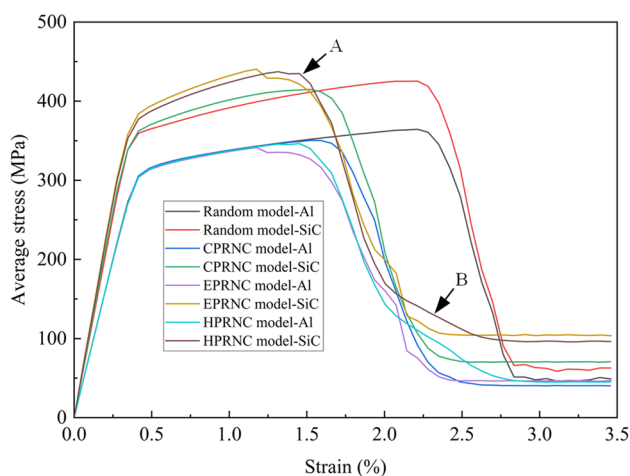

Fig. 9 Average stress of SiC particles and matrix in SiCp/Al

Effects of network particle distribution on cutting behavior of SiCp/Al

Figure 10 shows the cutting removal process of three network models. As shown in Fig. 10(a), when the tool is close to the network layer, the matrix material slides upward along the rake face and cracks are generated, and the particles show obvious stress concentration. Due to the extrusion of the matrix material, the interface between the circular and elliptical particles begins to fail, resulting in voids between the matrix and the particles. At the same time, the shear band of the EPRNC model is along the long axis of the elliptical particles, so the chip formation is earlier. As the tool moves, the chip is formed and separated from the workpiece material. As shown in Fig. 10(a, c), in the CPRNC model and the HPRNC model, the particles above the cutting path roll with the formation of chips. When the moving particles meet the particles in front of them, they will interact with each other, resulting in particle breakage. In addition, as shown in Fig. 10(b), in the EPRNC model, when the tool acts on the elliptical particles with a certain angle between the cutting path and the cutting direction, the particles are broken, and the machined surface will also produce smaller pits. At this time, a deep stress area is generated in the elliptical particles perpendicular to the machined surface. As the cutting progresses, as shown in Fig. 10(a, c), the particles below the cutting path are embedded in the machined surface under the extrusion of the tool flank, and no fracture occurs, thus forming a better machined surface quality. As shown in Fig. 10(b), in the EPRNC model, the tool interacts with particles perpendicular to the machined surface, and the particles deflect along the cutting direction and break in the middle and lower parts, resulting in deeper pit defects on the machined surface. At the same time, the particles in the subsurface region also produce more serious stress concentration. This shows that the particles with large aspect ratio are more likely to produce stress concentration and interface debonding during the cutting process. In addition, it can be seen from Fig. 9 that the mixed distribution of circular and elliptical particles makes the distribution of elliptical particles more dispersed, which reduces the mutual extrusion between elliptical particles and is conducive to improving cutting performance.

The above analysis shows that the network area with dense particles will result in a high stress concentration during the cutting process. The aggregation of particles with a high aspect ratio expands the EPRNC model's stress concentration range, and there is also a high stress concentration below the machined surface. The removal mode is greatly influenced by particle position relative to the cutting path and angle with the cutting direction. Large pits on the machined surface of the EPRNC model are caused by the high degree of fracture of elliptical particles. CPRNC
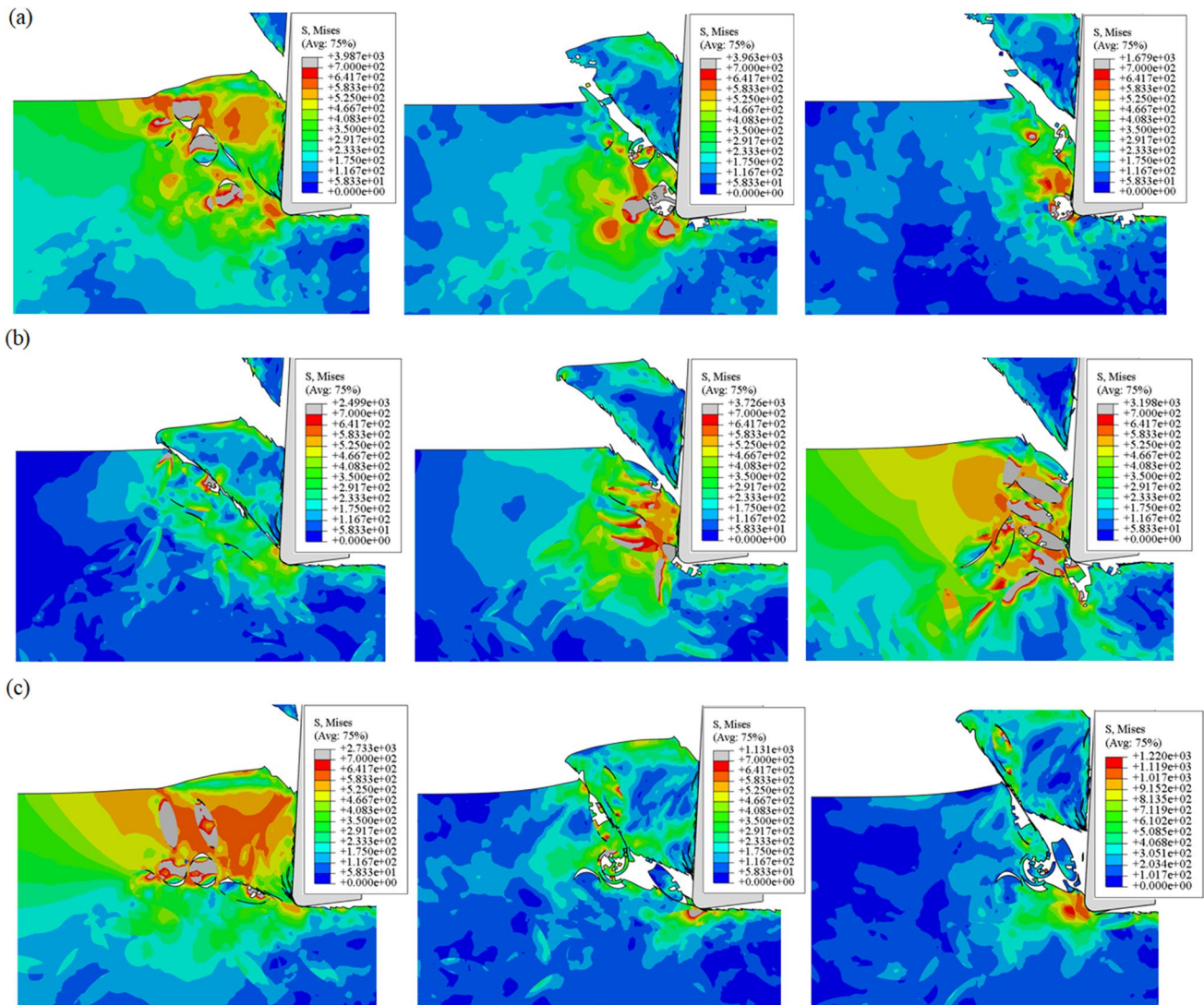
Fig. 10 Material removal process of network model: (**a**) CPRNC model, (**b**) EPRNC model, (**c**) HPRNC model

and HPRNC models, on the other hand, do not produce a wide range of stress concentration, and the defect depth of the machined surface is smaller, resulting in better surface quality.

Figure 11 shows the time-dependent variation of the cutting force of the four composites at a cutting depth of 0.05 mm. The exact location of the cutting force region on the model has been marked in Fig. 11. The graph shows that the fluctuation of cutting force is significant when cutting SiCp/Al. The fluctuation degree of cutting force of network composites increases noticeably when compared to randomly distributed composites. Multiple peaks in the cutting force curve are the result of chip formation and particle extrusion during the cutting process. Due to the unique structure of the network composites, when the tool cuts the matrix area, the formation of the chip will be hindered by

the front network layer. The deformation of the matrix will lead to interface debonding and particle breakage at the edge of the network layer, and the resistance of the tool is large. When the tool cuts the particles in the network layer, the direct contact between the tool and the particles causes the cutting force to increase sharply to the peak, as shown in Fig. 11(b, c, d). The peak cutting force of the network composites is greater than that of the randomly distributed composites, as shown in Fig. 12. This is because when the tool passes through the network layer, serious tool-particle and particle-particle interactions occur, and the cutting resistance of the tool increases, resulting in an increase in the cutting force of the tool. The cutting force peak of the EPRNC model is greater than that of other composites due to the more severe tool-particle interaction and stress concentration when cutting elliptical particles, as shown in
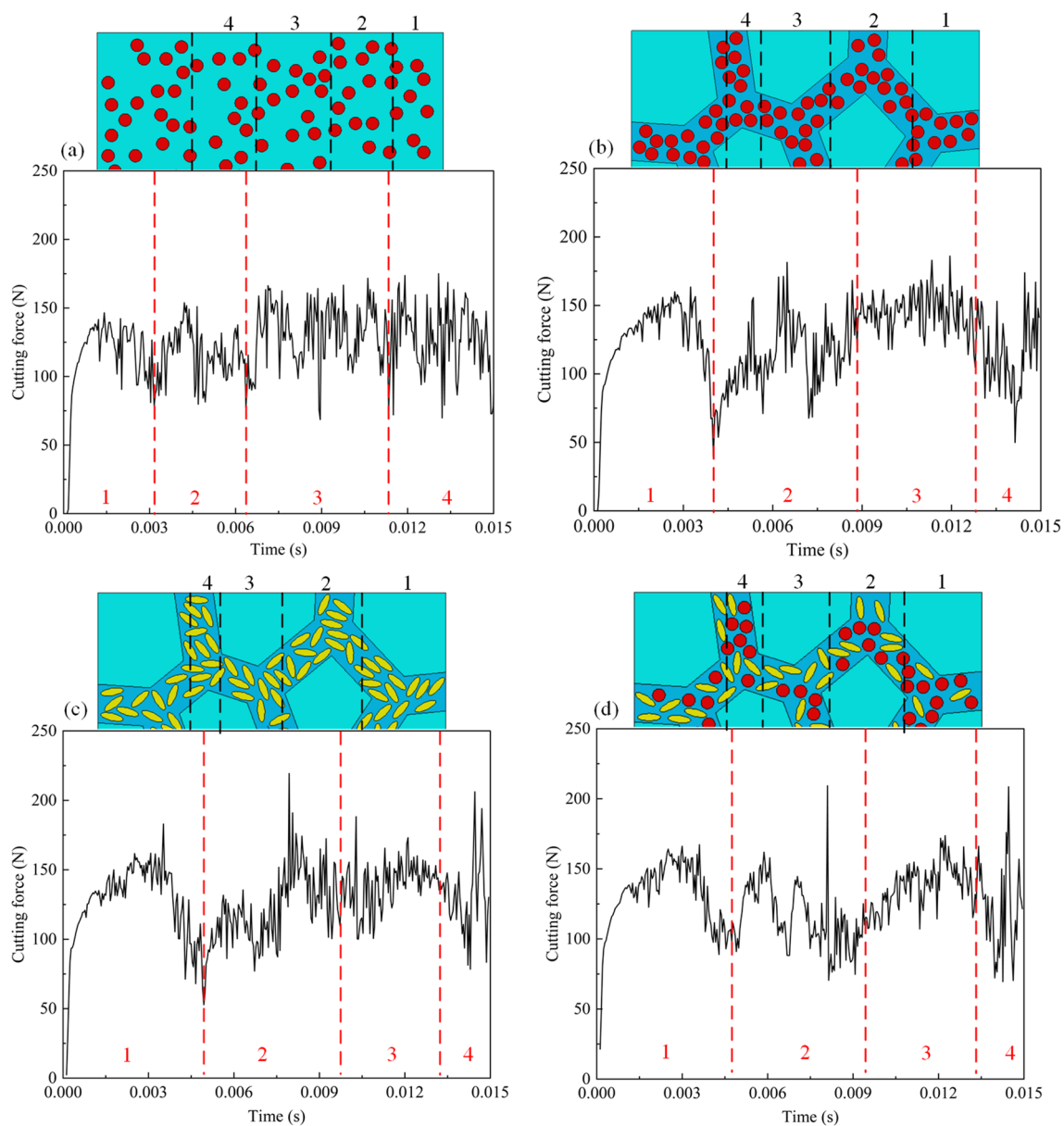
Fig. 11 Characteristics of cutting force of SiCp/Al at cutting depth of 0.05 mm: (**a**) random model, (**b**) CPRNC model, (**c**) EPRNC model, and (**d**) HPRNC model

Fig. 11(c). However, due to the presence of particles with a high aspect ratio, the average and peak cutting force of the HPRNC model is second only to the EPRNC model.

Figure 13 shows the machined surface morphology of random and network models when the cutting depth is 0.03 mm. Due to the random distribution of particles in the matrix, the defect positions on the machined surface of the random model (Fig. 13(a)) due to particle removal are also randomly distributed. Differently, the machined surface defects of the network model are concentrated in the network layer area. From Fig. 13(b, c), it can be seen that the scratches left by particle rolling and the tearing effect

on the matrix caused by the mutual extrusion of particles are the main reasons for the formation of large pit defects on the machined surface. As shown in Fig. 13(c), the elliptical particles deflect to a large extent during the cutting process, resulting in more serious particle fracture and interface debonding below the machined surface of the EPRNC model, which is attributed to the increase of the aspect ratio of the particles and the stronger tool-particle interaction. As shown in Fig. 13(d), defects caused by circular particles and elliptical particles are distributed on the machined surface of the HPRNC model, but the damage depth is small and the surface integrity is better.
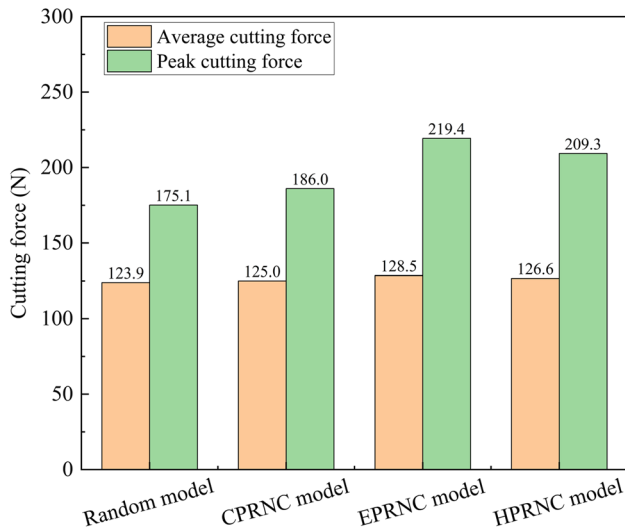
Fig. 12 Average and peak cutting forces

In order to quantitatively analyze the machined surface quality, the SSD depth of each model is marked with a black dotted line in Fig. 13. Figure 14 shows the SSD depth of the four models when the cutting depth is 0.03 mm. It can be seen that the SSD depth of the EPRNC model composed of elliptical particles with an aspect ratio of 3:1 is significantly larger than that of other models. Compared with the CPRNC model, the SSD depth of the EPRNC model is increased by 60.9%, which indicates that the EPRNC model will produce large subsurface damage and poor surface quality during processing, that is, increasing the aspect ratio of particles is unfavorable to cutting. In contrast, the machined subsurface damage of the HPRNC model is smaller. Although elliptical particles exist in the network structure, the SSD depth of the HPRNC model is reduced by 41.7% compared with the EPRNC model, indicating that the network composite material composed of circular and elliptical particles can obtain better cutting surface quality. Therefore, in the structural design of the network distribution SiCp/Al, it can be considered to improve the cutting performance and surface quality by mixing SiC particles with different aspect ratios.

The above analysis of the mechanical properties and cutting behavior of the network SiCp/Al demonstrates that the strengthening effect of the network structure composed of particles with a high aspect ratio on the composites is limited, and the elongation of the composites is likely to be sacrificed. In contrast, the hybrid particle network structure performs better. As a result, the uniaxial loading results will be used to guide reinforcement selection and network structure design. The shape of the reinforcement and the change in network structure will have an effect on the cutting performance of the composites. Furthermore, particles with a high aspect ratio will generate a lot of stress and surface defects during the cutting process, lowering the processing performance of the composites. To improve the mechanical and cutting properties of network composites, the particle composition and use of hybrid particles should be considered.

Conclusion

Tensile and cutting simulations of SiCp/Al composites with network and random distributions are performed, and the effects of network particle distribution on the mechanical properties and cutting of the composites are investigated. The following findings are made:
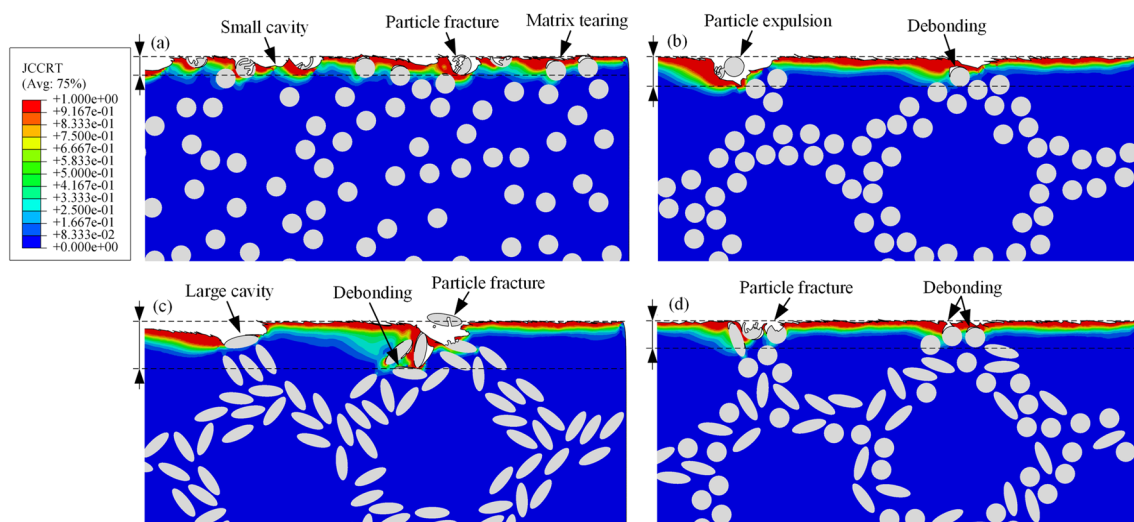

Fig. 13 Machined surface profiles of the four composites models: (**a**) random model, (**b**) CPRNC model, (**c**) EPRNC model, and (**d**) HPRNC model
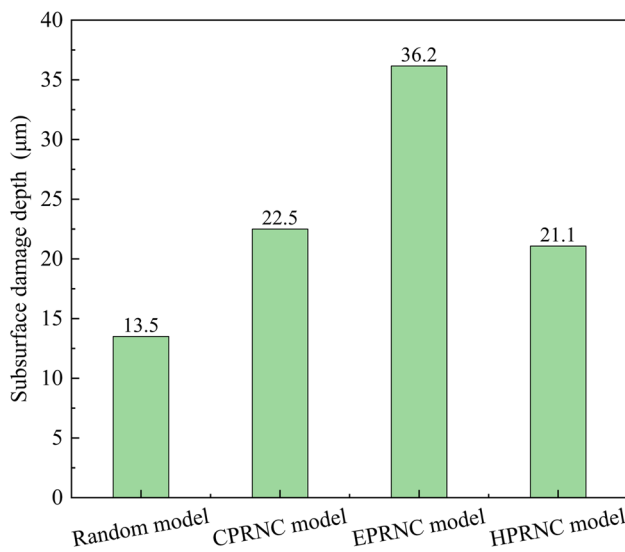
Fig. 14 Comparison of SSD depth of the four composites models

(1) When enhancer particles are distributed in a netlike pattern in the matrix, their carrying capacity is higher than when they are randomly distributed. This is due to the high continuity of the particles in the network layer, which allows the stress generated during the tensile process to be more easily transferred to the particles.

(2) When the reinforced particles are distributed in a network in the matrix, increasing the aspect ratio is advantageous to improve particle bearing capacity. With the increase in the content of ellipse particles in the composite network structure, the bearing capacity of particles also rises. This is because after the addition of ellipse particles, the continuity of particles is strengthened, allowing metal internal stresses to be more effectively transferred to particles. Ellipse particles have a longer interface, which facilitates the development of stress concentrations, but also increases the risk of particle fractures. The HPRNC model and the EPRNC model have comparable average stresses on particles within the small elastic deformation range, suggesting that the HPRNC model can achieve a bearing performance similar to that of the EPRNC model. And the particle stress distribution is more uniform in the hybrid particle network structure, and the plastic benefit of the matrix can be better employed.

(3) The fluctuation of the cutting force of the network composites is increased by the aggregation distribution of the reinforced particles in the network layer, and the cutting force is higher than that of the randomly distributed composites. The cutting force will rise sharply to the peak due to contact between the tool and the particles in the network layer. The interaction between the tool and the particles, as well as the stress concen-

tration, rise as the aspect ratio of the particles increases, resulting in an increase in cutting force.

(4) Particles with a higher aspect ratio will deflect and move more during the cutting process, resulting in severe pits and interface debonding on the subsurface. The network structure of hybrid particles with various aspect ratios has excellent uniform dispersion characteristics, reducing the interaction between particles. The cavities formed on the processing surface due to particle debonding are reduced. Compared with the network structure of ellipse particles, while maintaining the enhancing effect, the integrity of the processing surface is improved, and the depth of subsurface damage is reduced by 41.7%.

Future work

This work investigates the impact of improving the aspect ratio of particles on the strength and processing performance of metal matrix composites (MMCs), and explains its mechanism of action. Through the use of networks composed of both round and elliptical particles, a balance between strength and processing quality is achieved. This effort helps to expand the application range of aluminum-based metal matrix composites in aviation, automotive, military, and other fields. However, the optimal aspect ratio and the respective proportions of round and elliptical particles in the network structure on the properties of aluminum-based metal matrix composites still need to be studied.

Declarations

References

1. Deng B, Peng F, Zhou L, Liu M, Yang M, Yan R (2018) Analytical model of cutting force in micromilling of particle-reinforced metal matrix composites considering Interface failure. J Manuf Sci E T ASME 140. https://doi.org/10.1115/1.4040263
2. Kannan S, Kishawy HA (2007) Tribological aspects of machining aluminium metal matrix composites. J Mater Process Technol 198:399–406. https://doi.org/10.1016/j.jmatprotec.2007.07.021
3. El-Gallab M, Sklad M (1998) Machining of Al/SiC particulate metal matrix composites part II: Workpiece surface integrity. J Mater Process Technol 83:277–285. https://doi.org/10.1016/S0924-0136(98)00072-7
4. Kumar D, Singh PK, Saini P (2022) Morphological and mechanical characterization of the Al-4032/granite powder composites.

J Compos Mater 56:2433–2442. https://doi.org/10.1177/00219983221092837

5. Saini P, Singh PK (2022) Studies on microstructural characteristics and mechanical properties of hybrid Al-4032 AMC reinforced with SiC and granite marble powder. Proc Inst Mech Eng C J Mech Eng Sci 236:6192–6203. https://doi.org/10.1177/09544062211065342

6. Huang L, Geng L, Peng H-X (2015) Microstructurally inhomogeneous composites: is a homogeneous reinforcement distribution optimal? Prog Mater Sci 71:93–168. https://doi.org/10.1016/j.pmatsci.2015.01.002

7. Peng H-X, Fan Z, Mudher DS, Evans J (2002) Microstructures and mechanical properties of engineered short fibre reinforced aluminium matrix composites. Mater Sci Eng A 335:207–216. https://doi.org/10.1016/S0921-5093(01)01930-X

8. Kumai S, Hu J, Higo Y, Nunomura S (1996) Effects of dendrite cell size and particle distribution on the near-threshold fatigue crack growth behaviour of cast Al-SiCp composites. Acta Mater 44:2249–2257. https://doi.org/10.1016/1359-6454(95)00357-6

9. Huang LJ, Geng L, Li AB, Yang FY, Peng HX (2009) In situ TiBw/Ti–6Al–4V composites with novel reinforcement architecture fabricated by reaction hot pressing. Scr Mater 60:996–999. https://doi.org/10.1016/j.scriptamat.2009.02.032

10. Kaveendran B, Wang G, Huang L, Geng L, Luo Y, Peng H (2013) In situ (Al3Zrp+Al2O3np)/2024Al metal matrix composite with controlled reinforcement architecture fabricated by reaction hot pressing. Mater Sci Eng A 583:89–95. https://doi.org/10.1016/j.msea.2013.07.002

11. Gao X, Zhang X, Li A (2019) Numerical study on mechanical properties of quasi-continuous SiCp/Al network composites with various particle size ratios (PSRs). Int J Appl Mech 11:1950065. https://doi.org/10.1142/S1758825119500650

12. Slipenyuk A, Kuprin V, Milman Y, Spowart JE, Miracle DB (2004) The effect of matrix to reinforcement particle size ratio (PSR) on the microstructure and mechanical properties of a P/Mprocessed AlCuMn/SiCp MMC. Mater Sci Eng A 381:165–170. https://doi.org/10.1016/j.msea.2004.04.040

13. Monaghan J, Brazil D (1998) Modelling the flow processes of a particle reinforced metal matrix composite during machining. Compos A: Appl Sci Manuf 29:87–99. https://doi.org/10.1016/S1359-835X(97)00047-X

14. Kilickap TE, Çakır O (2008) Investigation of mechanical and machinability properties of SiC particle reinforced Al-MMC. J Mater Process Technol 198:220–225. https://doi.org/10.1016/j.jmatprotec.2007.06.082

15. Geni M, Kikuchi M (1998) Damage analysis of aluminum matrix composite considering non-uniform distribution of SiC particles. Acta Mater 46:3125–3133. https://doi.org/10.1016/S1359-6454(98)00004-4

16. Mishnaevsky LL (2004) Three-dimensional numerical testing of microstructures of particle reinforced composites. Acta Mater 52:4177–4188. https://doi.org/10.1016/j.actamat.2004.05.032

17. Dai W, Wang D, Chen G (2021) Mechanism of an approach based on bone microstructure to improve the machining quality for bionic multi-size particulate-reinforced composite. Compos Struct 274. https://doi.org/10.1016/j.compstruct.2021.114346

18. Zhou X, Gao Y, Wang Y, Xiao P (2023) Comparison of mechanical properties of 2024Al composites strengthened with the carbon fibers and/or ZrC particles. J Mater Sci 58:7930–7947. https://doi.org/10.1007/s10853-023-08530-3

19. Ghandehariun A, Kishawy HA, Umer U, Hussein HM (2015) Analysis of tool-particle interactions during cutting process of metal matrix composites. Int J Adv Manuf Technol 82:143–152. https://doi.org/10.1007/s00170-015-7346-1

20. Teng X, Chen W, Huo D, Shyha I, Lin C (2018) Comparison of cutting mechanism when machining micro and nano- particles reinforced SiC/Al metal matrix composites. Compos Struct 203:636–647. https://doi.org/10.1016/j.compstruct.2018.07.076

21. Jin P, Gao Q, Wang Q, Li W (2021) Micro-milling mechanism and surface roughness of high volume fraction sicp/al composites. Int J Adv Manuf Technol 115:91–104. https://doi.org/10.1007/s00170-021-07129-9

22. Zhang P, Yue X, Zhang Q, Zong C, Fang Y (2021) Investigation on the influence of sic particle parameters on the machinability of SiCp/Al composite. Vacuum 191. https://doi.org/10.1016/j.vacuum.2021.110340

23. Saini P, Singh PK (2022) Effect of machining parameters on surface roughness and energy consumption during end milling of stir cast Al-4032/6%SiC composite. Surf Topogr Metrol Prop 10:035029. https://doi.org/10.1088/2051-672X/ac8d1c

24. Saini P, Singh PK (2022) Investigation on characterization and machinability of Al-4032/SiC metal matrix composite. Surf Topogr Metrol Prop 10:025007. https://doi.org/10.1088/2051-672X/ac5de4

25. Saini P, Singh PK (2022) Experimental investigation on microstructure, mechanical and machining properties of Al-4032/granite marble powder (GMP) composite produced through stir casting. Materialwissenschaft Werkst 53:1450–1467. https://doi.org/10.1002/mawe.202200078

26. Prasad VVB, Bhat BVR, Mahajan YR, Ramakrishnan P (2002) Structure-property correlation in discontinuously reinforced aluminium matrix composites as a function of relative particle size ratio. Mater Sci Eng A 337:179–186. https://doi.org/10.1016/S0921-5093(02)00024-2

27. Zhao S, Xu Y, Pan C, Liang L, Wang X (2019) Microstructural modeling and strengthening mechanism of TiB/Ti-6Al-4V discontinuously-reinforced titanium matrix composite. Materials 12:827. https://doi.org/10.3390/ma12050827

28. Yu W, Chen J, Ming W, An Q, Chen M (2021) Experimental and FEM study of cutting mechanism and damage behavior of ceramic particles in orthogonal cutting SiCp/Al composites. Ceram Int 47:7183–7194. https://doi.org/10.1016/j.ceramint.2020.11.072

29. Zhou L, Cui C, Zhang P, Ma Z (2016) Finite element and experimental analysis of machinability during machining of high-volume fraction SiCp/Al composites. Int J Adv Manuf Technol 91:1–10. https://doi.org/10.1007/s00170-016-9933-1

30. Hooputra H, Gese H, Gese H, Werner H (2004) A comprehensive failure model for crashworthiness simulation of aluminium extrusions. Int J Crashworthines 9:449–464. https://doi.org/10.1533/ijcr.2004.0289

31. Hillerborg A, Modeer M, Peterson PE (1976) Analysis of crack formation and crack growth in concrete by means of fracture. Cem Concr Res 6:773–782. https://doi.org/10.1016/0008-8846(76)90007-7

32. Wang Y, Liao W, Yang K, Chen W, Liu T (2019) Investigation on cutting mechanism of SiCp/Al composites in precision turning. Int J Adv Manuf Technol 100:963–972. https://doi.org/10.1007/s00170-018-2650-1

33. Xu W, Yiquan L, Jinkai X, Huadong Y, Wei L (2020) Comparison and research on simulation models of aluminum-based silicon carbide micro-cutting. Int J Adv Manuf Technol 109:1–17. https://doi.org/10.1007/s00170-020-05518-0